Case 3. $N < m < \infty$: When $m > N$, the transmitter may receive an ACK from each receiver before all the m copies are transmitted. Let $Q_j(K)$ denote the probability that all the K receivers successfully receive the data block in j copies

$$Q_j(K) = [1 - (1 - P_s)^j]^K \qquad (4)$$

Let $R_j(K)$ denote the probability that the K receivers receive the data block successfully exactly at the jth copy

$$R_j(K) = Q_j(K) - Q_{j-1}(K) \qquad (5)$$

Then $L(m)$ can be evaluated by

$$L(m) = \sum_{j=1}^{m-N} R_j(K)(j + N - 1) + m \sum_{j=m-N+1}^{m} R_j(K) + \sum_{i=0}^{K-1} \binom{K}{i} [1 - (1 - P_s)^m]^i \times [(1 - P_s)^m]^{K-i}[m + 2(N - 1) + S(P_s, K - i)] \qquad (6)$$

Numerical results and discussions: Fig. 1 shows the throughput efficiencies of the MSR, MGBN, Morris's scheme, and the optimal scheme among the investigated ones against P_s

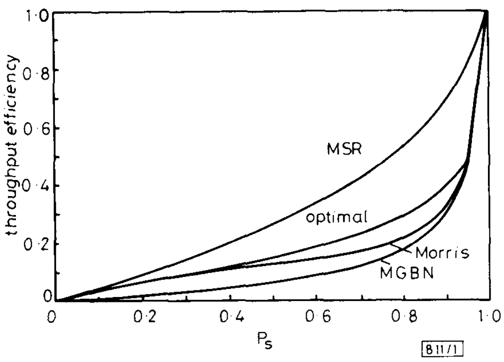

Fig. 1 *Throughput efficiency against* P_s
$N = 5; K = 5$

for $N = 5$ and $K = 5$. The throughput efficiencies of the MSR, MGBN and Morris's schemes are equal to $1/S(P_s, K)$, $1/[1 - N + NS(P_s, K)]$ and $1/[(N - 1)(1 - P_s^K) + S(P_s, K)]$, respectively. One can see that the optimal scheme provides a significant improvement in throughput efficiency over Morris's scheme for $P_s \in [0.4, 0.9]$. The percentage of improvement is about 31% at $P_s = 0{\cdot}85$.

Figs. 2 and 3 shows similar results for $N = 10$, $K = 5$ and $N = 5$, $K = 20$, respectively. Comparing Figs. 1, 2 and 3. one can see that the improvement is more significant when N and/or K are larger. In reality, the improvement at $P_s = 0.85$ is about 101% and 74% for $N = 10$, $K = 5$ and $N = 5$, $K = 20$, respectively.

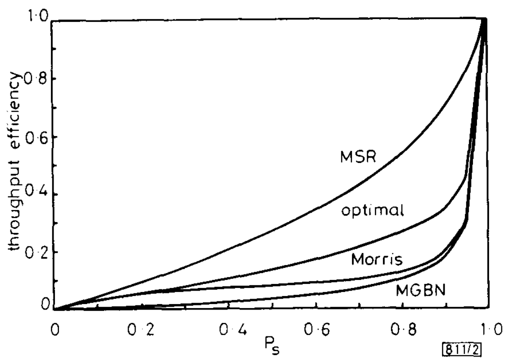

Fig. 2 *Throughput efficiency against* P_s
$N = 10; K = 5$

There are several interesting topics in this area that can be studied further. For example, it is worth evaluating the performance of various ARQ schemes for multidestination

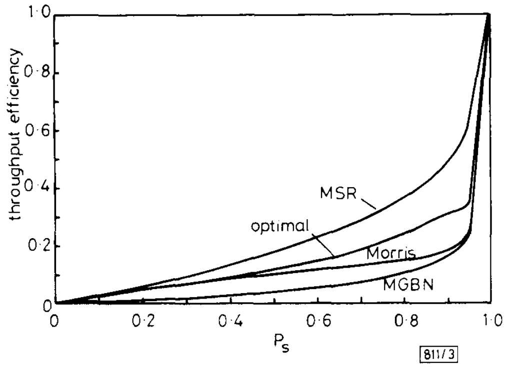

Fig. 3 *Throughput efficiency against* P_s
$N = 5; K = 20$

environments where round-trip delays between the transmitter and different receivers are not the same.

T-H. LEE *18th July 1990*

Department of Communication Engineering
National Chiao Tung University
Hsinchu, Taiwan 30050
Republic of China

References

1 GOPAL, I. S., and JAFFE, J. M.: 'Point-to-multipoint communication over broadcast links', *IEEE Trans.*, 1984, **COM-32**, pp. 1034–1044
2 MASE, K., TAKENNAKA, T., YAMAMOTO, H., and SHINOHARA, M.: 'Go-back-N ARQ schemes for point-to-multipoint satellite communications', *ibid.*, 1983, **COM-31**, pp. 583–590
3 SABNANI, K., and SCHWARTZ, M.: 'Multidestination protocols for satellite broadcast channels', *ibid.*, 1985, **COM-33**, pp. 232–239
4 MOENECLAEY, M., and BRUNEEL, H.: 'Efficient ARQ scheme for high error rate channels', *Electron. Lett.*, 1984, **20**, pp. 986–987
5 SASTRY, A. R. K.: 'Improving automatic repeat-request (ARQ) performance on satellite channels under high error rate conditions', *IEEE Trans.*, 1975, **COM-23**, pp. 436–439
6 MORRIS, J. M.: 'On another go-back-N ARQ technique for high error rate conditions', *ibid.*, 1978, **COM-26**, pp. 187–189
7 CHO, Y. J., and UN, C. K.: 'Continuous multidestination ARQ schemes for high error-rate channels', *Electron. Lett.*, 1988, **24**, pp. 694–695

TWO-BAND IIR QUADRATURE MIRROR FILTER DESIGN

Indexing term: Filters

Two types of two-band IIR quadrature mirror filter structure are proposed. The aliasing distortion and amplitude distortion can be exactly cancelled. The Remez exchange algorithm is used iteratively to optimise the filter response, which results in an equal-ripple design.

Introduction: Quadrature mirror filters (QMF) have great applications in sub-band coding systems.[1,2] In general, a sub-band coding system suffers from three kinds of distortions: aliasing distortion, amplitude distortion and phase distortion. If a sub-band coding system is free from these three distortions, it is called a 'perfect reconstruction' system. Theoretically, only FIR filter banks can achieve perfect reconstruction.[3] Ordinary FIR filters have large transition band. If both a sharp transition band and reasonable stop-band attenuation are required, one must use very high order

FIR filters. In VLSI implementation, high order means that a large amount of multipliers are required. Our alternative approach is using lower order IIR filters to achieve sharp transition band and good stopband attenuation. We propose two IIR QMF structures. The aliasing distortion and amplitude distortion are inherently cancelled by the special system characteristics, leaving phase distortion. The filter response is optimised by the Remez exchange algorithm, which results in an equal-ripple design.

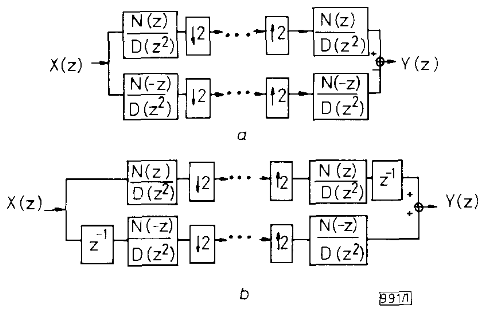

Fig. 1 *Two band IIR QMF structures*

IIR QMF Structures: Fig. 1*a* shows the first system structure. Note that the analysis filter and the synthetis filter are the same. The numerator $N(z)$ is constrained to be a linear phase filter of order M, the denominator $D(z^2)$ will be derived from $N(z)$ to make the system have no amplitude distortion. From the structure in Fig. 1, we can write the input/output relation as

$$Y(z) = \frac{1}{2}\left[X(z)\frac{N(z)}{D(z^2)} + X(-z)\frac{N(-z)}{D(z^2)}\right]\frac{N(z)}{D(z^2)} - \frac{1}{2}\left[X(z)\frac{N(-z)}{D(z^2)} + X(-z)\frac{N(z)}{D(z^2)}\right]\frac{N(-z)}{D(z^2)} = \frac{1}{2}\cdot\frac{N(z)^2 - N(-z)^2}{D(z^2)^2}\cdot X(z) \quad (1)$$

Note that the aliasing term $X(-z)$ is automatically cancelled. Thus the system transfer function can be written as

$$T(z) = \frac{1}{2}\cdot\frac{N(z)^2 - N(-z)^2}{D(z^2)^2} \quad (2)$$

Since even order terms of $N(z)^2 - N(-z)^2$ are eliminated, eqn. 2 can be rewritten as

$$T(z) = \frac{1}{2}\cdot\frac{P(z^2)z^{-1}}{D(z^2)^2} \quad (3)$$

where $P(z)$ is a linear phase filter of order $M - 1$. Now we decompose $P(z)$ into a minimum phase filter $P_{min}(z)$ and a maximum phase filter $P_{max}(z)$. Their relations are

$$P(z) = P_{min}(z)\cdot P_{max}(z) \quad (4a)$$

$$P_{max}(z) = P_{min}(z^{-1})\cdot z^{-(M-1)/2} \quad (4b)$$

$$|P_{min}(e^{j\omega})|^2 = |P_{max}(e^{j\omega})|^2 = |P(e^{j\omega})| \quad (4c)$$

If we select

$$D(z) = P_{min}(z)/\sqrt{2} \quad (5)$$

Then the amplitude distortion will be cancelled, since by eqns. 3–5

$$|T(e^{j\omega})| = \frac{1}{2}\cdot\frac{|P(e^{j2\omega})\cdot e^{j\omega}|}{|P_{min}(e^{j2\omega})|^2\cdot\frac{1}{2}} = \frac{|P(e^{j2\omega})|}{|P_{min}(e^{j2\omega})|^2} = 1 \quad (6)$$

eqn. 4*b* also implies that M must be odd (i.e., even length).

The second structure is shown in Fig. 1*b*, which is slightly different from Fig. 1*a*. An unit delay is inserted in each channel. The two channels are added, not subtracted. With the same procedure as above, we obtain the following relations:

$$Y(z) = \frac{1}{2}\left[X(z)\frac{N(z)}{D(z^2)} + X(-z)\frac{N(-z)}{D(z^2)}\right]\frac{N(z)}{D(z^2)}\cdot z^{-1} + \frac{1}{2}\left[X(z)\frac{N(-z)}{D(z^2)}\cdot z^{-1} + X(-z)\frac{N(z)}{D(z^2)}\cdot(-z^{-1})\right]\frac{N(-z)}{D(z^2)} = \frac{1}{2}\cdot\frac{N(z)^2 + N(-z)^2}{D(z^2)^2}\cdot z^{-1}\cdot X(z) \quad (7)$$

$$T(z) = \frac{1}{2}\cdot\frac{N(z)^2 + N(-z)^2}{D(z^2)^2}\cdot z^{-1} \quad (8)$$

Since odd order terms of $N(z)^2 + N(-z)^2$ are eliminated, eqn. 8 can be rewritten as

$$T(z) = \frac{1}{2}\cdot\frac{P(z^2)\cdot z^{-1}}{D(z^2)^2} \quad (9)$$

where $P(z)$ is a linear phase filter of order M. $P(z)$ is decomposed into $P_{min}(z)$ and $P_{max}(z)$, which are related by

$$P_{max}(z) = P_{min}(z^{-1})\cdot z^{-m/2} \quad (10)$$

Select $D(z)$ as eqn. 5, then the amplitude distortion will be cancelled as eqn. 6. Eqn. 10 also implies that M must be even (i.e., odd length).

Design method and examples: The relation between $N(z)$ and $D(z)$ has been derived. Next we have to design $N(z)$ such that $[N(z)/D(z^2)]$ is an optimal lowpass filter with sharp transition band. Our method iteratively uses the Remez exchange algorithm to optimise $N(z)$. Suppose $N_k(z)$ is the design result in the kth iteration, then $D_k(z)$ can be obtained by eqn. 5. Using $D_k(z)$ as a weighting function, we can design $N_{k+1}(z)$ by optimising $[N_{k+1}(z)/D_k(z^2)]$, and calculate $D_{k+1}(z)$ by eqn. 5. This procedure is iteratively run until a given criterion is reached. The initial condition is $D_0(z) = 1$. The frequency band to optimise is $\{0\} \cup [\omega_c, \pi]$, where $\omega_c > \pi/2$ is the stopband cutoff frequency. The desired value and weighting function are given by

$$N(e^{j\omega}) = 1 \quad \text{weighting} = 1000 \quad \omega = 0 \quad (11a)$$

$$N(e^{j\omega}) = 0 \quad \text{weighting} = \frac{1}{D(e^{j2\omega})} \quad \omega \in [\omega_c, \pi] \quad (11b)$$

where eqn. 11*a* forces $N(e^{j0})$ to be unity. Since the transition band $(0, \omega_c)$ of $N(z)$ is very large, the stopband ripple would be very small which implies that

$$|P(e^{j2\omega})| = |N(e^{j\omega})^2 + N(-e^{j\omega})^2| > 0 \quad \text{for any } \omega$$

So all roots of $P(z)$ would be either inside or outside the unit circle, with none on the unit circle. Therefore all roots of

Table 1 DESIGN PARAMETERS AND RESULTS FOR STRUCTURE

Design parameters: $M = 9$, $\omega_c = 0{\cdot}51\pi$

	$N(z)$	$D(z)$
0	0·01376882455503996	0·1326548219222183
1	0·04021034876968750	0·3573434336738553
2	0·09493226529643952	0·3405581267025623
3	0·1499292429152811	0·1323795827496087
4	0·1909745171609607	0·01669443234657305
5	0·1909745171609607	
6	0·1499292429152811	
7	0·09493226529643952	
8	0·04021034876968750	
9	0·01376882455503996	

Iterations = 16

Amplitude response $|T(e^{j\omega})|$: 1·0000000000 ~ 1·0000000005

$P_{min}(z)$ are inside unit circle and stability is guaranteed. No proof is given for convergence, but we have checked many examples and found that all examples converge very quickly, except for ω_c very close to $\pi/2$.

Table 2 DESIGN PARAMETERS AND RESULTS FOR STRUCTURE B

Design parameters: $M = 8$, $\omega_c = 0{\cdot}51\pi$

	$N(z)$	$D(z)$
0	0·02182177645752444	0·1634194967253134
1	0·05654791855163643	0·3912458990346937
2	0·1247719859429595	0·3143143780978576
3	0·1767738313263649	0·09182630156619157
4	0·2062465455764888	0·005827822717659886
5	0·1767738313263649	
6	0·1247719859429595	
7	0·05654791855163643	
8	0·02182177645752444	

Iterations = 17
Amplitude response $|T(e^{i\omega})|$: 1·0000000000 ~ 1·0000000001

Table 1 lists an example for odd M. Table 2 lists another example for even M. Both examples are completed in less than 20 iterations. From the total amplitude response it is clear that amplitude distortion is cancelled. Only the frequency response of Table 1 is given in Fig. 2. From Fig. 2, we know

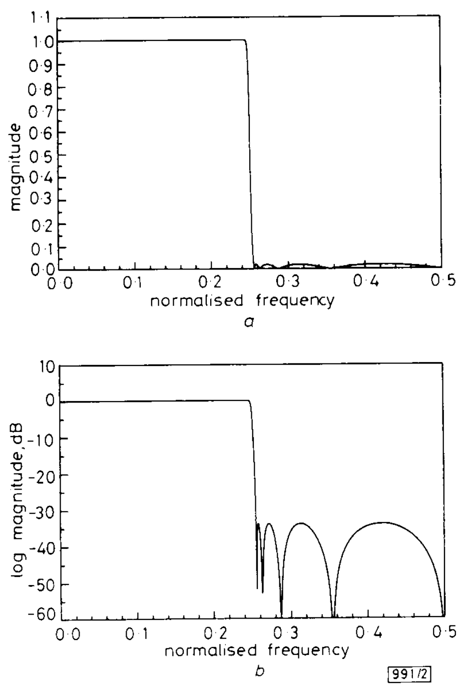

Fig. 2 *Frequency response of $N(z)/D(z^2)$ in Table 1*

that the result is an equal-ripple design. Sharp transition band and high stopband attenuation are also achieved as shown in Fig. 2*a*.

S.-B. JAW
S.-C. PEI

Department of Electrical Engineering
National Taiwan University
Taipei, Taiwan, Republic of China

19th March 1990

References

1 ESTEBAN, D., and GALAND, C.: 'Application of quadrature mirror filters to split-band voice coding schemes'. Proc. IEEE ICASSP 1977, pp. 191–195

2 BARNWELL, T. P.: 'Subband coder design incorporating recursive quadrature filters and optimum ADPCM coders', *IEEE Trans.*, 1982, **ASSP-30**, pp. 751–765

3 VAIDYANATHAN, P. P.: 'Theory and design of M-channel maximally decimated quadrature mirror filters with arbitrary M, having the perfect-reconstruction property', *IEEE Trans.*, 1987, **ASSP-35**, pp. 476–492

ROOM TEMPERATURE IR PHOTODETECTOR WITH ELECTROMAGNETIC CARRIER DEPLETION

Indexing terms: Photodetectors, Semiconductor devices and materials

The practical implementation of ambient temperature InSb electromagnetically carrier-depleted (EMCD) IR photodetectors is reported. The device is a lightly doped InSb photoconductor with a high backside surface recombination velocity, placed in a magnetic field. The carrier concentration in the most part of the device is highly reduced because of the action of the Lorentz force. This results in saturation of the I/V characteristics and the possible suppression of Auger recombination. The practical EMCD InSb photoconductor has been manufactured and characterised. The saturation of the I/V characteristic and the increase of photoresponse by a factor of ~10 has been achieved using a static electrical field of ~30 V/cm and a magnetic field of about 1·5 T. The EMCD devices promise fast photodetectors with high responsivity operating at room temperature.

Introduction: One of the main goals of the recent efforts on IR photodetectors is the increase of the temperature of operation to the ambient temperature with simultaneous preservation of near BLIP performance.[1–6] The main obstacle to achieving this ultimate goal is the large level of noise caused by Auger generation. As the Auger generation is proportional to the carrier concentration, it can be reduced to low values by decreasing the carrier concentration below equilibrium values.

Elliott and Ashley proposed methods to suppress the Auger generation. These methods were based on phenomena known in semiconductor physics—the minority carrier exclusion at n^+n junctions and combination of carrier exclusion and extraction in n^+vp^+ structures.[1–5] Although the practical devices have been demonstrated,[5] it is difficult to achieve the potential performance in practice. The problems arise from requirements of high quality semiconductor structures with complicated doping/gap profiles, high bias power dissipation, large flicker noise and other requirements.

We propose the suppression of the Auger generation by depletion of the semiconductor using the well-known magnetoconcentration effect.[7–11] The magnetoconcentration effect has been studied in detail in the literature. We propose its use for ambient temperature photodetectors with significant Auger generation.

The practical realisation of this principle requires a lightly doped semiconductor with a weak Shockley-Read recombination rate, and a low and a high surface recombination velocities at the front and back surface. The device should be designed to dissipate a power density of about 1 W/mm^2 without significant increase of the semiconductor temperature.

Experimental: Fig. 1 shows geometry of the EMCD photoconductor. The preparation of the device is quite similar to the standard preparation of photoconductors from narrow gap semiconductors.[12] The main differences in preparation are the special treatment of the surfaces. The surface recombination velocity should be high at the back side and as low as possible at the front side. It is also necessary to achieve good heat dissipation. The lightly doped InSb of both n and p type, with a concentration of about 10^{14} cm^{-3} has been used. The preparation of the active elements includes

(*a*) Preparation of back surface. The flat back surface with a high surface recombination velocity has been obtained by